Dual-gel 4D Printing of Bioinspired Tubes

Jiayu Liu[1], Ozan Erol[1,2,3], Aishwarya Pantula[3], Wangqu Liu[3], Zhuoran Jiang[3], Kunihiko Kobayashi[9], Devina Chatterjee[3], Narutoshi Hibino[5], Lewis H. Romer[6,7], Sung Hoon Kang[1,2,8], Thao D. Nguyen[1,2] and David H. Gracias[3,4,]*

[1] Department of Mechanical Engineering, Johns Hopkins University, 3400 N Charles Street, Baltimore, MD 21218, USA
[2] Hopkins Extreme Materials Institute, 3400 N Charles Street, Baltimore,Johns Hopkins University, Baltimore, MD 21218, USA
[3] Department of Chemical & Biomolecular Engineering, Johns Hopkins University, 3400 N Charles Street, Baltimore,Baltimore, MD 21218, USA
[4] Department of Materials Science and Engineering, Johns Hopkins University, 3400 N Charles Street, Baltimore, Baltimore, MD 21218, USA
[5] Division of Cardiac Surgery, Department of Surgery, 1800 Orleans Street, Johns Hopkins Hospital, Baltimore, MD 21287, USA
[6] Departments of Anesthesiology and Critical Care Medicine, Cell Biology, Pediatrics, Johns Hopkins University School of Medicine, 1800 Orleans Street, Baltimore, MD 21287, USA
[7] Biomedical Engineering and the Center for Cell Dynamics, Johns Hopkins University School of Medicine, 1800 Orleans Street, Baltimore, MD 21287, USA
[8] Institute for NanoBioTechnology, Johns Hopkins University, 3400 N Charles Street, Baltimore, Baltimore, MD 21218, USA
[9] JSR Corporation, 1-9-2, Higashi-Shimbashi, Minato-ku, Tokyo 105-8640, Japan

*Corresponding author: dgracias@jhu.edu

KEYWORDS: biomedical engineering, stimuli-responsive polymers, 3D printing, soft robotics, implants

ABSTRACT

The distribution of periodic patterns of materials with radial or bilateral symmetry is a universal biological design principle. Amongst the many biological forms, tubular shapes are a common motif in many organisms, and they are also important for bioimplants and soft robots. However, the simple design principle of strategic placement of 3D-printed segments of swelling and non-swelling materials to achieve widely different functionality has yet to be demonstrated. Here, we report the design, fabrication, and characterization of segmented 3D printed gel tubes composed of an active thermally responsive swelling gel (poly N-isopropylacrylamide; pNIPAM) and a passive thermally non-responsive gel (polyacrylamide; pAAM). Using finite element simulations and experiments, we report the variety of shape changes including uniaxial elongation, radial expansion, bending, and gripping based on two gels. Actualization and characterization of thermally induced shape changes are of key importance to robotics and biomedical engineering. Our studies present rational approaches to engineering complex parameters with a high level of customization and tunability into additive manufacturing of dynamic gel structures.

INTRODUCTION

The radial or bilateral distribution of chemicals during growth and morphogenesis is a widely observed feature in biology, seen in more than 99% of modern animals, and across diverse species ranging from humans to microorganisms.[1] Tubular biological species and their functional components including nematodes, flowers, marine animals and elephant trunks also show symmetric and/or periodic arrangements of different material segments. The organisms exploit the swelling mismatch and mechanical instabilities inherent in these structures to enable complex shape change and motion. It is noteworthy that tubular shapes are essential in human engineering due to the need for bioimplants such as vascular grafts[2] and continuum robots.[3] Apart from static designs, controllable shape change in tubular shapes such as elongation, lumen expansion and bending could facilitate smart or autonomous behaviors, but such features are challenging to incorporate especially in an unwired, external-power-free, and customizable manner.[4,5]

Stimuli-responsive polymers offer significant opportunities for implementing a range of smart, adaptive and dynamic behaviors in response to temperature, light, electromagnetic fields, and chemicals.[6–12] As one of the most widely used stimuli-responsive materials, thermally responsive poly N-isopropylacrylamide (pNIPAM) has been utilized to create a range of shape-changing structures including grippers,[13,14] propellers,[15,16] and actuators.[17–19] When coupled with 3D printing, a high level of customization, tunability and adaptability can be achieved.

4D printing which introduces a new dimension of time[20–26] has been previously utilized to create shape-changing structures and devices.[27–40] Besides the well-recognized advantage of easy programmability as a path-based additive manufacturing method, 3D printing also offers excellent potential in material integration and switching of dissimilar materials on demand (in a manner that is analogous to weaving). Among the different types of 3D printing, direct ink writing (DIW) of gels has notable advantages over alternative 3D gel

printing methods such as stereolithography in terms of low cost implementation and the ease of incorporating multiple gels at the same time.

Inspired by symmetrical and periodic tubular structures in biology and motivated by the need to create untethered, thermally responsive bioimplants and continuum robots, we explored the 4D printing of tubes with alternating segmental patterns of an active thermoresponsive gel (poly N-isopropylacrylamide; pNIPAM) and a passive thermally non-responsive gel (polyacrylamide; pAAM) based on direct ink writing. The essential challenge in our work was to elucidate, rationalize and validate design principles by which sequential arrangements of segments of high and low swelling stimuli-responsive gels could elicit dramatically different shape change of functional importance.

The similar acrylamide composition of the gels is essential to ensure interfacial adhesion in segmented designs. First, printable inks were made by blending monomers of these gels with a clay (Laponite) that alters the rheological characteristics of the gels and enables shear thinning behaviors. Using finite element modeling and bioinspiration, we generated standard tessellation language (STL) to make tubes with different periodic vertical and horizontal arrangement of active and passive segments that could generate a diverse range of shape changes including uniaxial elongation, bending, radial expansion, and gripping. Further, inspired by coral polyps, we designed and printed tubes with self-folding fingers at one end, and these structures display more complex dual-function thermally responsive shape change involving both uniaxial expansion of the tube and finger gripping. We anticipate that this novel bioinspired approach utilizing segmented placement of active and passive stimuli-responsive materials, when combined with finite element simulations and the versatility of customizable 3D printing designs, offers the possibility of producing a range of multi-functional shape-changing structures with broad applicability.

MATERIALS AND METHODS

Preparation of the active NIPAM and passive AAM inks:

Active NIPAM ink: Laponite XLG (Southern Clay Products) was first mixed with DI water using magnetic stirring, followed by a planetary mixer (Mazerustar KK-250S, Kurabo Industry Ltd.) 10 vol% of a 0.12 mg ml^{-1} solution of Methacryloxyethyl thiocarbamoyl Rhodamine B (Polysciences, Inc.) was used as the dye for fluorescence imaging. The aqueous dye solution was added to the Laponite solution and mixed with the planetary mixer. Subsequently, N-Isopropylacrylamide (NIPAM, Scientific Polymer Products Inc.) monomer and Irgacure 2959 (BASF) as a UV photoinitiator was added to the Laponite-dye solution and mixed again using the planetary mixer. The final concentrations (by weight) of each component in the active NIPAM ink were as follows: 84.6% DI water, 8.46% NIPAM,[21] 6.77% Laponite, 0.17% Irgacure, 0.001% Methacryloxyethyl thiocarbamoyl Rhodamine B. The NIPAM concentration was chosen based upon literature precedent and our empiric data.

Passive AAM ink: Laponite solution was prepared in the same way as the active ink. 10 vol% of a 0.3 mg ml^{-1} solution of Fluorescein o-methacrylate (97%, Sigma-Aldrich) was used as the dye for the passive ink. The dye solution also contained 2 mg ml^{-1} NaOH (Fisher Scientific) since the dye monomer is dissolvable in base conditions, and was mixed by magnetic stirring. Subsequently, acrylamide (AAM, Sigma-Aldrich) monomer, Irgacure 2959 and N,N′-methylenebisacrylamide (BIS, Sigma-Aldrich; BIS functions as a crosslinker) was added to the Laponite-dye solution and mixed using the planetary mixer. The final concentrations (by weight) of each component in the passive ink were: 82.97% DI water, 7.88% AAM, 6.64% Laponite, 0.83% Irgacure, 1.66% BIS, 0.0025% Fluorescein o-methacrylate, 0.017% NaOH.

3D printing of pNIPAM and pAAM dual-hydrogel modules:

The NIPAM and AAM inks were loaded into syringes, transferred to UV-shielded cartridges and centrifuged to remove any bubbles present in the cartridges. The inks were kept at room

temperature for at least 24 hrs to allow thorough hydration needed to achieve the desired shear thinning properties. The cartridges were then attached to the Direct Ink Writing 3D Printer (Inkredible+ 3D Bioprinter, Cellink) and connected to an air pump pressure control. We chose nozzles 22G (diameter 0.41 mm) which ensures smooth and clog-free printing. All the computer-aided-design (CAD) and STL files were generated in Solidworks (Dassault Systèmes). Then, the G-code for each design was generated using the software Slic3r (layer height 0.4 mm, printing speed 10 mm s^{-1}). Before printing the final designs, we printed test structures to calibrate the two printing nozzles so that they were perfectly aligned with each other. The structures were printed on silicon wafers at room temperature in air. The printing pressures were optimized for each ink to ensure smooth printing at a speed of 10 mm s^{-1}. The pressures used for printing active and passive inks were 90-100 kPa and 110-130 kPa, respectively.

UV photocuring:

After 3D printing, we photocured the structures using an Omnicure UV source (LX 500, Lumen Dynamics). We designed a rotating platform that rotates slowly at 9.6 rpm to enable relatively uniform exposure of UV light and consequently uniform curing of gel tubes (see details in Note S1). Two UV LED heads with 365 nm wavelength were used to cure the tubular structures, and we used a lens of diameter 12mm for each UV LED head and a resulting intensity of 0.4 W/cm^2 at a distance of 3 cm. We cured the tubular structures with 100% power and section by section depending on the structural height. Each section was cured for 9 mins using two UV LED heads at the same time. UV absorbance spectra of the inks and FTIR spectra of the structures before and after curing are in Figure S10.

Rheological characterization of the inks:

The rheology of the inks was measured using a rheometer (Modular Compact Rheometer MCR 302, Anton Paar, Austria) with a 1^o cone-plate geometry. The temperature of the plate

was kept at 23°C. Ink viscosities were measured via a logarithmic sweep of shear rates ranging from 0.01 s^{-1} to 1000 s^{-1}. Oscillatory experiments were performed at a constant frequency of 1 Hz.

Mechanical characterization of the 3D printed and photocured hydrogels:

Active and passive hydrogel square plates with a side length of 10 mm and a thickness of 2 mm were 3D printed and UV cured using the methods described above. After curing, the hydrogel samples were kept in DI water at room temperature for 24 hours so that they could reach their equilibrium swollen state. We used DMA (Dynamic Mechanical Analyzer Q800, TA Instruments) to conduct unconfined compression tests on the samples in air. Three samples were tested for each hydrogel and the engineering stress - strain curves were calculated (Figure S3). Young's moduli of the active and passive hydrogels were calculated from slopes of the engineering stress–engineering strain curves.

Macro-imaging:

All optical images were taken with a digital camera (Canon EOS 70D) and a broad spectrum UV light source (Spectroline Model EF-160C, Spectronics Corporation, USA) to excite the fluorescent dyes in the inks. The images of photocured tubes were taken at room temperature in air after UV curing. Then, the structures were placed in DI water and put into an incubator (MODEL 1575, Sheldon Manufacturing, INC., USA) set at the desired temperatures for 24 hours to reach the equilibrium swollen state at each temperature. The photographs of transformed structures were taken in DI water.

RESULTS AND DISCUSSION

Development of active and passive hydrogel inks and 3D printing of homogeneous tubes

To be 3D printed via Direct Ink Writing (DIW), a material must display unique rheological or shear thinning characteristics.[41,42] Hence, the first step was to create thermoresponsive and non-thermoresponsive NIPAM and AAM inks for DIW. pNIPAM has a lower critical solution temperature (LCST) above which it transforms from a hydrophilic to hydrophobic state and expels water with a significant reduction in volume.[43] pAAM lacks the critical isopropyl group and shows no LCST.

Both NIPAM and AAM have previously been printed using stereolithography[25] and DIW.[20,21,23,24] We blended the monomer NIPAM with different shear-thinning agents including Xanthan Gum, Gellan Gum, and Laponite nanoclay. All of the three agents showed shear-thinning properties (the rheology measurements of our NIPAM inks are shown in Figure S1) and could be printed by direct ink writing. We attribute this observation to dissociation of the ink network under applied shear stress. Consequently, the ink could be extruded out of the printing nozzle, and when the shear stress was removed after printing the network reassembled and the extruded ink retained its shape.[41]

We observed however, that the Laponite-blended ink had a higher storage modulus than the other two inks (modulus measurements for NIPAM inks are shown in Figure S1(B)), and could be used to print taller structures. The AAM-blended inks showed similar rheological and modulus trends. Therefore, we chose Laponite as the shear-thinning agent for both our active NIPAM and passive AAM inks. Also, a free radical curing agent Irgacure was added to both inks to facilitate photocuring with ultraviolet (UV) light. It has been previously reported, and we confirmed, that the Laponite-NIPAM-Irgacure mixture was photocrosslinkable and retained its shape in water.[44,45] However, it was necessary to add a crosslinker, N,N′-methylenebis(acrylamide) (BIS) - to the AAM inks, so that they did not dissolve in water after printing and curing (Figure S2).

Printing dual material 3D structures presents unique challenges even with the two-nozzle printer used in our experiments (see Note S1 on experimental set-up). Briefly, we developed a calibration methodology to reduce misalignment between nozzles during the approximately 50-100 print layers required for our structures (experimental details in Note S1). We also designed a rotary photocuring stage to ensure homogeneous crosslinking of the pNIPAM and pAAM gels. After printing and photocuring in air, the structures were soaked in deionized (DI) water which induced swelling and releasing from the substrate. The conceptual schematic of the 4D Printing process is shown in **Figure 1A**.

We first verified the swelling of the active pNIPAM, and nonswelling of the passive pAAM by measuring the diameter change of homogeneously printed single component pNIPAM and pAAM tubes by placing them in DI water at different temperatures (25^{o}C, 33^{o}C, 41^{o}C, and 50^{o}C) where they were allowed to reach an equilibrium shape over 24 hours (**Figure 1B**). We observed dramatic increases (38%) and decreases in the diameter ($\Delta D/D_0$) of the pNIPAM tubes on cooling and heating, respectively, while there was no significant change (1.2%) in the diameter of pAAM tubes. This swelling behavior agrees with prior swelling data from photolithographically patterned pNIPAM and pAAM gels.[9,46] Consequently, we consider the pNIPAM portion of the structure to be the active gel that drives shape change by swelling or deswelling, while the pAAM portion is largely passive. We attribute the hysteresis to a variety of factors including reorganization of chains of crosslinked and uncrosslinked polymer, as well as documented differences in intra- and intermolecular hydrogen bonding that occur between heating and cooling.[47-49]

Mechanical properties and calibration of the finite element model

As discussed previously, symmetric composite materials are widely found in nature. When the constituent materials have different mechanical properties such as the extent of swellability in our two gels, this can lead to predictable and controllable shape change, that is

amenable to modeling by finite element methods. We applied finite element analysis (FEA) to guide the design of symmetric 3D gel tubes (Details in the Note S2). Briefly, in our hydrogel constitutive model, the free energy of the hydrogel is assumed to be the sum of a mechanical part, represented by a quasi-incompressible Neo-Hookean model for the entropy elasticity of the polymer network with Gaussian chain statistics, and a component for the energy of mixing between polymer network and solvent, represented by the Flory−Huggins model. We focused on the hydrogel equilibrium shape change for each test temperature and implemented our equilibrium model into the open-source finite element code TAHOE (Sandia National Laboratories). The simulation starts from the photocured state, and we determined the final tube shape at different temperatures by changing the Flory- Huggins parameter in the active hydrogel to achieve the experimentally measured swelling (**Figure 1B**) and then solved for the displacement field.

We measured Young's moduli of 3D printed and photocured pNIPAM and pAAM square plates using a Dynamic Mechanical Analyzer and found them to be 2.53 kPa and 60.3 kPa, respectively (**Figure S3**). Using these modulus values and measured volumetric swelling from the completely dry to the equilibrium swollen state at room temperature (Note S2), the Flory-Huggins interaction parameter was obtained by fitting the swelling of homogeneous pNIPAM and pAAM tubes obtained from the model to that measured in the experiments during heating (**Figure 1B**). We applied these parameters to the finite element model for predicting the complex shape transformation of the dual-gel tubes (Note S3 and Figure S4).

4D printing of symmetrically patterned tubes

Applying the FEA model and experiments, we explored the rational design of shape-changing gel tubes by the symmetric placement of horizontal (**Figure 2**) or vertical (**Figure 3**) segments of active pNIPAM gels interspaced with passive pAAM gels. After 3D printing and photocuring, the structures were soaked in DI water at 25^{o}C, 35^{o}C, and 50^{o}C for 24 hours to

reach the equilibrium state. Bilaterally symmetric tubes with equally spaced, alternating cylindrical-disk-shaped segments of pNIPAM (three segments), and pAAM (four segments) showed elongation as high as 32%, with good agreement between FEA simulations and experiments (**Figure 2A-B** and Figure S5). As compared with homogeneous tubes of pNIPAM that elongate by approximately the same extent (38%, **Figure 1B**), the introduction of passive segments constrained radial expansion of the tube, so that its predominant shape change was uniaxial elongation.

When the same number of alternating pNIPAM and pAAM segments were placed at angles with respect to each other (**Figure 2C-D** and Figure S6), like cylindrical wedges, the tube bent by approximately 25^{o}. The bending angle decreased as we increased temperature, and at 50^{o}C, it reversed to the photocured state (θ = 0^{o}), in agreement with simulation snapshots.

We next printed tubes with twelve alternating vertical segments of pNIPAM and of pAAM (six of each), on top of a constraining ring of pAAM. The tubes expanded radially by 75% but did not elongate. Constrained by the nonswelling strips of pAAM, the tube buckled and folded downwards to accommodate the elongation of the pNIPAM strips by swelling (**Figure 3A-B** and Figure S7). The tubes recovered their original shapes when we increased the temperature to 50^{o}C.

We also designed tubes with wedge-shaped alternating pNIPAM and pAAM vertical segments and overhanging pNIPAM "fingers" constrained by pAAM edges. The pNIPAM "fingers" are more constrained at their bottoms than at their tops. As a result, the "fingers" bent by approximately, ω = 35^{o} when the pNIPAM gel swelled at 25^{o}C (**Figure 3C-D**, Figure S7).

3D printed dual shape-change tubes

Advanced biomedical or soft robotics applications often require a library of parts that may transform in shape. Nature is replete with such complex shape-change organisms. For example, the coral polyp is an aquatic animal with a cylindrical vase-shaped body with radially distributed tentacles capable of capturing prey (**Figure 4A**).[50] Our design, simulation, and 3D printing approach is amenable to the creation of such complex shape-change devices. Inspired by the coral polyp, we designed dual shape-change tubes, composed of a uniaxial elongation tubular base (**Figure 2A**) and a bending three finger gripper module (**Figure 3C**). A 3D printed passive ring at the bottom of the base served as a handle (**Figure 4B-C**). After 3D printing and photocuring, the structure was suspended in air on top of a cuboidal object placed at the bottom of the tank (**Figure 4D**). When the tank was filled with water at 25^{o}C, the polyp-inspired tube showed two shape-change events by simultaneously elongating and bending its fingers to grab onto the cube (**Figure 4E**). It is noteworthy that the fingers were able to firmly grasp the cube so that it could be lifted from the bottom of the tank (**Figure 4F**). Upon heating to 50^{o}C, the fingers opened up, the base contracted and the cube was released (**Figure 4G**).

CONCLUSION

We utilized bioinspired principles of symmetric arrangements of high-swelling and low-swelling gels in tubular geometries to achieve uniaxial elongation, radial expansion, bending, and gripping. The use of symmetry and segments combined with numerical modeling enables rational design of shape-changing primitives and their combinations to produce significantly complex motions of practical importance. We designed a dual-function tube capable of simultaneous elongation and gripping inspired by coral polyp; this polyp inspired tube can reach into a tank and grab an object (Snapshots are shown in Figure S8). We incorporated advanced multi-material integration in the direct ink writing process to achieve

interweaving of active and passive materials with a 3D structure and with a high spatial resolution of approximately 400 microns. Additive manufacturing with multi-material integration permits direct printing of the assembly of shape-changing primitives and potentially of functional grading. It is conceivable that this approach could be extended to the 4D printing of more complicated assemblies, including those with soft and rigid segments[51] or those with multiple temperature responsive gels[52] to enable sequential motions for more complicated tasks. For example, shape-changing tubular constructs which elongate, bend or increase in size are important for pediatric tissue and vascular implants to accommodate and adjust to the effects of growth of the surrounding tissues.[53,54] Alternatively, tubes that elongate and grip are important for soft-robotic endoscopic applications.[55] Coupling our methodology with materials that respond to alternative and/or additional stimuli such as biochemicals,[9] light,[56] or magnetic fields[38,57] would further enhance programmability and complexity, and facilitate realization of multistage, goal-oriented control of broad relevance to soft-robotics and biomedical engineering.

ASSOCIATED CONTENT

Supporting Information

Detailed methods for 3D printing of the dual-gel modules. Details of finite element analysis, parameters for constitutive model, mechanical properties measurement of inks and photocured gels, and time lapse of tubes shape change. This material is available free of charge via the Internet at http://pubs.acs.org

AUTHOR INFORMATION

Corresponding Author

*E-mail: dgracias@jhu.edu

Present Address

[3]Department of Chemical & Biomolecular Engineering, Johns Hopkins University, 3400 North Charles Street, Baltimore, MD 21218, USA

Author Contributions

D.H.G., T.D.N., S.H.K., L.H.R., and N.H. conceived of the study and supervised the experiments and simulations. J.L., K.K., O.E., A.P., W.L., Z.J., D.C. conducted the experiments and. J.L. carried out the simulations. J.L., T.D.N and D.H.G. wrote the manuscript with input and edits from all authors.

Acknowledgements
Research reported in this publication was supported by the Eunice Kennedy Shriver National Institute of Child Health & Human Development of the National Institutes of Health under Award Number R21HD090663. We also acknowledge support from the National Science Foundation (NSF DMR-170349, EFMA-1830893) and Johns Hopkins University start-up fund. We acknowledge V. Nagal and Dr. A. Ghosh for assistance with the FTIR measurements and UV-Vis measurements respectively. The content is solely the responsibility of the authors and does not necessarily represent the official views of the funding agencies.

Notes
The authors declare no competing interests.

REFERENCES

(1) Finnerty, J. R.; Pang, K.; Burton, P.; Paulson, D.; Martindale, M. Q. Origins of Bilateral Symmetry: Hox and Dpp Expression in a Sea Anemone. *Science* **2004**, *304* (5675), 1335–1337.
(2) Murphy, S. V.; Atala, A. 3D Bioprinting of Tissues and Organs. *Nat. Biotechnol.* **2014**, *32* (8), 773–785.
(3) Jones, B. A.; Walker, I. D. Kinematics for Multisection Continuum Robots. *IEEE Trans. Rob.* **2006**, *22* (1), 43–55.
(4) Rus, D.; Tolley, M. T. Design, Fabrication and Control of Soft Robots. *Nature* **2015**, *521* (7553), 467–475.
(5) Whitesides, G. M. Soft Robotics. *Angew. Chem. Int. Ed Engl.* **2018**, *57* (16), 4258–4273.
(6) Ahn, S.-K.; Kasi, R. M.; Kim, S.-C.; Sharma, N.; Zhou, Y. Stimuli-Responsive Polymer Gels. *Soft Matter* **2008**, *4* (6), 1151.
(7) Tokarev, I.; Minko, S. Stimuli-Responsive Hydrogel Thin Films. *Soft Matter* **2009**, *5* (3), 511–524.
(8) Stuart, M. A. C.; Huck, W. T. S.; Genzer, J.; Müller, M.; Ober, C.; Stamm, M.; Sukhorukov, G. B.; Szleifer, I.; Tsukruk, V. V.; Urban, M.; Winnik, F.; Zauscher, S.;Luzinov, I.; Minko, S. Emerging Applications of Stimuli-Responsive Polymer Materials. *Nat. Mater.* **2010**, *9* (2), 101–113.
(9) Gracias, D. H. Stimuli Responsive Self-Folding Using Thin Polymer Films. *Curr. Opin. Chem. Eng.* **2013**, *2* (1), 112–119.
(10) Jeon, S.-J.; Hauser, A. W.; Hayward, R. C. Shape-Morphing Materials from Stimuli-Responsive Hydrogel Hybrids. *Acc. Chem. Res.* **2017**, *50* (2), 161–169.
(11) Cangialosi, A.; Yoon, C.; Liu, J.; Huang, Q.; Guo, J.; Nguyen, T. D.; Gracias, D. H.; Schulman, R. DNA Sequence-Directed Shape Change of Photopatterned Hydrogels via High-Degree Swelling. *Science* **2017**, *357* (6356), 1126–1130.
(12) Kuksenok, O.; Singh, A.; Balazs, A. C. Designing Polymer Gels and Composites That Undergo Bio-Inspired Phototactic Reconfiguration and Motion. *Bioinspir. Biomim.* **2018**, *13* (3), 035004.
(13) Wang, E.; Desai, M. S.; Lee, S.-W. Light-Controlled Graphene-Elastin Composite Hydrogel Actuators. *Nano Lett.* **2013**, *13* (6), 2826–2830.
(14) Breger, J. C.; Yoon, C.; Xiao, R.; Kwag, H. R.; Wang, M. O.; Fisher, J. P.; Nguyen, T. D.; Gracias, D. H. Self-Folding Thermo-Magnetically Responsive Soft Microgrippers. *ACS Appl. Mater. Interfaces* **2015**, *7* (5), 3398–3405.
(15) Magdanz, V.; Stoychev, G.; Ionov, L.; Sanchez, S.; Schmidt, O. G. Stimuli-Responsive Microjets with Reconfigurable Shape. *Angew. Chem. Int. Ed Engl.* **2014**, *53* (10), 2673–2677.
(16) Huang, H.-W.; Sakar, M. S.; Petruska, A. J.; Pané, S.; Nelson, B. J. Soft Micromachines with Programmable Motility and Morphology. *Nat. Commun.* **2016**, *7*, 12263.
(17) Hauser, A. W.; Evans, A. A.; Na, J.-H.; Hayward, R. C. Photothermally Reprogrammable Buckling of Nanocomposite Gel Sheets. *Angew. Chem. Int. Ed Engl.* **2015**, *54* (18), 5434–5437.
(18) Lee, E.; Kim, D.; Kim, H.; Yoon, J. Photothermally Driven Fast Responding Photo-Actuators

Fabricated with Comb-Type Hydrogels and Magnetite Nanoparticles. *Sci. Rep.* **2015**, *5*, 15124.
(19) Zhou, Y.; Hauser, A. W.; Bende, N. P.; Kuzyk, M. G.; Hayward, R. C. Waveguiding Microactuators Based on a Photothermally Responsive Nanocomposite Hydrogel. *Adv. Funct. Mater.* **2016**, *26* (30), 5447–5452.
(20) Bakarich, S. E.; Gorkin, R.; Panhuis, M. in H.; Spinks, G. M. 4D Printing with Mechanically Robust, Thermally Actuating Hydrogels. *Macromol. Rapid Commun.* **2015**, *36* (12), 1211–1217.
(21) Gladman, A. S.; Matsumoto, E. A.; Nuzzo, R. G.; Mahadevan, L.; Lewis, J. A. Biomimetic 4D Printing. *Nat. Mater.* **2016**, *15* (4), 413–418.
(22) An, J.; Chua, C. K.; Mironov, V. A Perspective on 4D Bioprinting. *International Journal of Bioprinting* **2016**, *2* (0).
(23) Jin, Y.; Shen, Y.; Yin, J.; Qian, J.; Huang, Y. Nanoclay-Based Self-Supporting Responsive Nanocomposite Hydrogels for Printing Applications. *ACS Appl. Mater. Interfaces* **2018**, *10* (12), 10461–10470.
(24) Chen, T.; Bakhshi, H.; Liu, L.; Ji, J.; Agarwal, S. Combining 3D Printing with Electrospinning for Rapid Response and Enhanced Designability of Hydrogel Actuators. *Adv. Funct. Mater.* **2018**, *28* (19), 1800514.
(25) Han, D.; Lu, Z.; Chester, S. A.; Lee, H. Micro 3D Printing of a Temperature-Responsive Hydrogel Using Projection Micro-Stereolithography. *Sci. Rep.* **2018**, *8* (1), 1963.
(26) Zheng, S. Y.; Shen, Y.; Zhu, F.; Yin, J.; Qian, J.; Fu, J.; Wu, Z. L.; Zheng, Q. Programmed Deformations of 3D-Printed Tough Physical Hydrogels with High Response Speed and Large Output Force. *Adv. Funct. Mater.* **2018**, 1803366.
(27) Ge, Q.; Jerry Qi, H.; Dunn, M. L. Active Materials by Four-Dimension Printing. *Appl. Phys. Lett.* **2013**, *103* (13), 131901.
(28) Raviv, D.; Zhao, W.; McKnelly, C.; Papadopoulou, A.; Kadambi, A.; Shi, B.; Hirsch, S.; Dikovsky, D.; Zyracki, M.; Olguin, C.; Raskar, R.; Tibbits, S. Active Printed Materials for Complex Self-Evolving Deformations. *Sci. Rep.* **2014**, *4*, 7422.
(29) Ge, Q.; Dunn, C. K.; Jerry Qi, H.; Dunn, M. L. Active Origami by 4D Printing. *Smart Mater. Struct.* **2014**, *23* (9), 094007.
(30) Kokkinis, D.; Schaffner, M.; Studart, A. R. Multimaterial Magnetically Assisted 3D Printing of Composite Materials. *Nat. Commun.* **2015**, *6*, 8643.
(31) Mao, Y.; Ding, Z.; Yuan, C.; Ai, S.; Isakov, M.; Wu, J.; Wang, T.; Dunn, M. L.; Qi, H. J. 3D Printed Reversible Shape Changing Components with Stimuli Responsive Materials. *Sci. Rep.* **2016**, *6*, 24761.
(32) Ge, Q.; Sakhaei, A. H.; Lee, H.; Dunn, C. K.; Fang, N. X.; Dunn, M. L. Multimaterial 4D Printing with Tailorable Shape Memory Polymers. *Sci. Rep.* **2016**, *6*, 31110.
(33) Teoh, J. E. M.; An, J.; Chua, C. K.; Lv, M.; Krishnasamy, V.; Liu, Y. Hierarchically Self-Morphing Structure through 4D Printing. *Virtual Phys. Prototyp.* **2016**, *12* (1), 61–68.
(34) Ding, Z.; Yuan, C.; Peng, X.; Wang, T.; Qi, H. J.; Dunn, M. L. Direct 4D Printing via Active Composite Materials. *Sci Adv* **2017**, *3* (4), e1602890.
(35) Momeni, F.; Seyed M Mehdi Hassani; Liu, X.; Ni, J. A Review of 4D Printing. *Mater. Des.* **2017**, *122*, 42–79.
(36) Teoh, J. E. M.; Zhao, Y.; An, J.; Chua, C. K.; Liu, Y. Multi-Stage Responsive 4D Printed Smart Structure through Varying Geometric Thickness of Shape Memory Polymer. *Smart Mater. Struct.* **2017**, *26* (12), 125001.
(37) Dutta, S.; Cohn, D. Temperature and pH Responsive 3D Printed Scaffolds. *J. Mater. Chem. B Mater. Biol. Med.* **2017**, *5* (48), 9514–9521.
(38) Leist, S. K.; Gao, D.; Chiou, R.; Zhou, J. Investigating the Shape Memory Properties of 4D Printed Polylactic Acid (PLA) and the Concept of 4D Printing onto Nylon Fabrics for the Creation of Smart Textiles. *Virtual Phys. Prototyp.* **2017**, *12* (4), 290–300.
(39) Basit, A. W.; Gaisford, S. *3D Printing of Pharmaceuticals*; Springer, 2018.
(40) Kim, Y.; Yuk, H.; Zhao, R.; Chester, S. A.; Zhao, X. Printing Ferromagnetic Domains for Untethered Fast-Transforming Soft Materials. *Nature* **2018**, *558* (7709), 274–279.
(41) Guvendiren, M.; Lu, H. D.; Burdick, J. A. Shear-Thinning Hydrogels for Biomedical Applications. *Soft Matter* **2012**, *8* (2), 260–272.
(42) Truby, R. L.; Lewis, J. A. Printing Soft Matter in Three Dimensions. *Nature* **2016**, *540* (7633),

371–378.
(43) Hirokawa, Y.; Tanaka, T. Volume Phase Transition in a Non-ionic Gel; 1984.
(44) Haraguchi, K.; Takehisa, T.; Fan, S. Effects of Clay Content on the Properties of Nanocomposite Hydrogels Composed of Poly(N-Isopropylacrylamide) and Clay. *Macromolecules* **2002**, *35* (27), 10162–10171.
(45) Wang, J.; Lin, L.; Cheng, Q.; Jiang, L. A Strong Bio-Inspired Layered PNIPAM-Clay Nanocomposite Hydrogel. *Angew. Chem. Int. Ed Engl.* **2012**, *51* (19), 4676–4680.
(46) Yoon, C.; Xiao, R.; Park, J.; Cha, J.; Nguyen, T. D.; Gracias, D. H. Functional Stimuli Responsive Hydrogel Devices by Self-Folding. *Smart Mater. Struct.* **2014**, *23* (9), 094008.
(47) Lu, Y.; Zhou, K.; Ding, Y.; Zhang, G.; Wu, C. Origin of Hysteresis Observed in Association and Dissociation of Polymer Chains in Water. *Physical Chemistry Chemical Physics* **2010**,12(13), 3188-94.
(48) Wu, C.; Wang, X. Globule-to-coil Transition of a Single Homopolymer Chain in Solution. *Physical Review Letters* **1998**, 80(18), 4092.
(49) Cheng, H.; Shen, L.; Wu, C. LLS and FTIR Studies on the Hysteresis in Association and Dissociation of Poly (N-isopropylacrylamide) Chains in Water. *Macromolecules* **2006**, 39(6), 2325-9.
(50) Chisholm, H. *Encyclopedia Britannica: A Dictionary of Arts, Sciences, Literature and General Information*; 1911.
(51) Guo, J.; Shroff, T.; Yoon, C.; Liu, J.; Breger, J. C.; Gracias, D. H.; Nguyen, T. D. Bidirectional and Biaxial Curving of Thermoresponsive Bilayer Plates with Soft and Stiff Segments. *Extreme Mechanics Letters* **2017**, *16*, 6–12.
(52) Kobayashi, K.; Oh, S. H.; Yoon, C.; Gracias, D. H. Multitemperature Responsive Self-Folding Soft Biomimetic Structures. *Macromol. Rapid Commun.* **2018**, *39* (4).
(53) Poynter, J. A.; Eghtesady, P.; McCrindle, B. W.; Walters, H. L., 3rd; Kirshbom, P. M.; Blackstone, E. H.; Husain, S. A.; Overman, D. M.; Austin, E. H.; Karamlou, T.; Lodge, A. J.; St Louis, J. D.; Gruber, P. J.; Ziemer, G.; Davies, R. R.; Jacobs, J. P.; Brown, J. W.; Williams, W. G.; Tchervenkov, C. I.; Jacobs, M. L.; Caldarone, C. A.; Congenital Heart Surgeons' Society. Association of Pulmonary Conduit Type and Size with Durability in Infants and Young Children. *Ann. Thorac. Surg.* **2013**, *96* (5), 1695–1701; discussion 1701–1702.
(54) Salem, A. M. Right Ventricle to Pulmonary Artery Connection: Evolution and Current Alternatives. *Journal of the Egyptian Society of Cardio-Thoracic Surgery* **2016**, *24* (1), 47–57.
(55) Patel, N.; Seneci, C. A.; Shang, J.; Leibrandt, K.; Yang, G.-Z.; Darzi, A.; Teare, J. Evaluation of a Novel Flexible Snake Robot for Endoluminal Surgery. *Surg. Endosc.* **2015**, *29* (11), 3349–3355.
(56) Liu, Y.; Boyles, J. K.; Genzer, J.; Dickey, M. D. Self-Folding of Polymer Sheets Using Local Light Absorption. *Soft Matter* **2012**, *8* (6), 1764–1769.
(57) Hu, W.; Lum, G. Z.; Mastrangeli, M.; Sitti, M. Small-Scale Soft-Bodied Robot with Multimodal Locomotion. *Nature* **2018**, *554* (7690), 81–85.

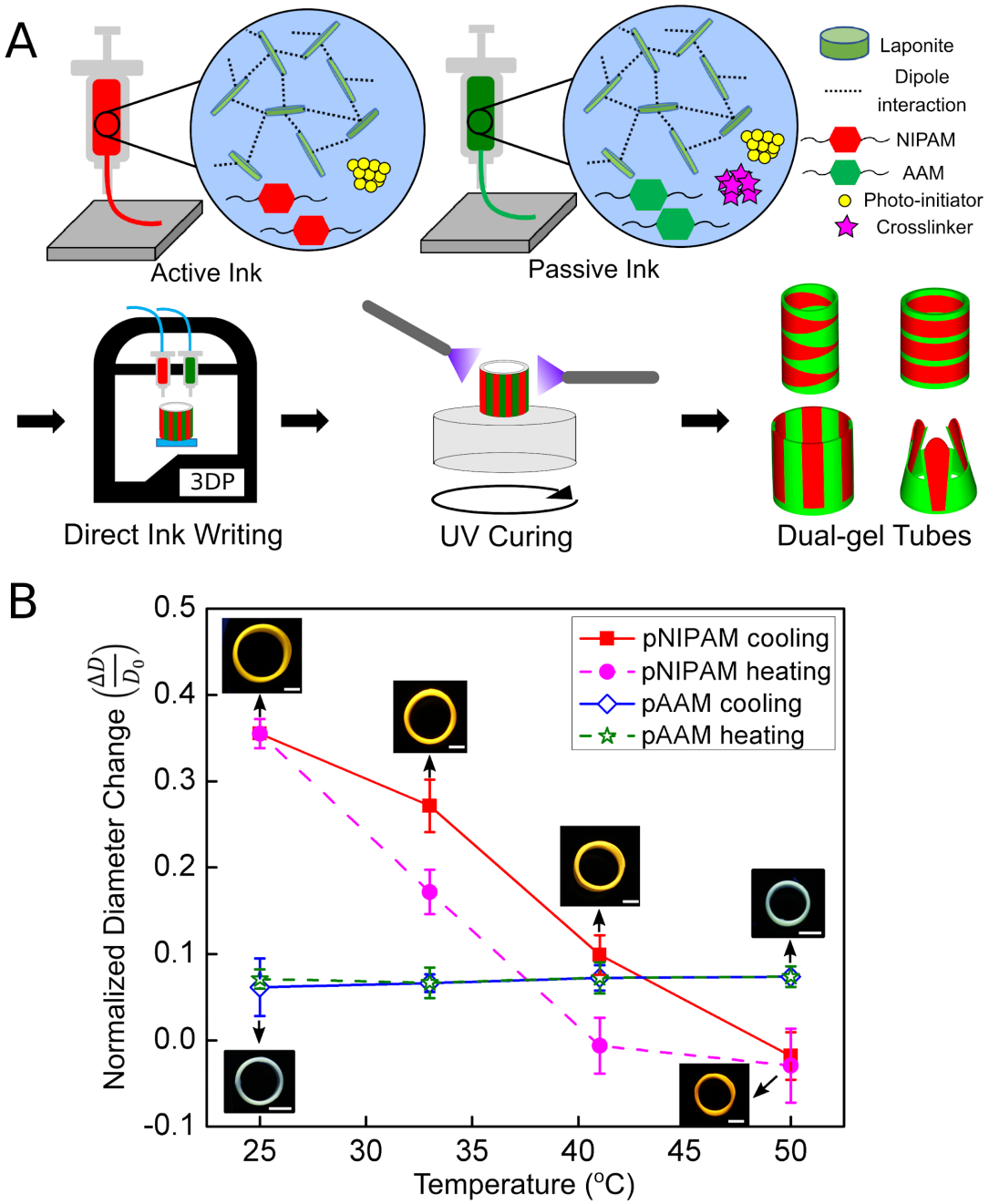

Figure 1. Schematics of the 4D Printing process and experimental characterization of the swelling of printed active and passive hydrogel tubes. (**A**) Schematic showing the microstructure of the active NIPAM and passive AAM inks and different steps in the process including formulation of the inks, 3D direct ink writing and photocuring. (**B**) A plot showing the experimentally measured normalized diameter change ($\Delta D/D_0$) in water at different temperatures between 25 °C and 50 °C for 3D printed and photocured tubes composed of pNIPAM and pAAM. D_0 is the diameter of the 3D printed and photocured tube in air. Bars indicate standard deviation with a sample size of three and data at each temperature was taken at equilibrium after 24 hours. Inset shows several snapshots of the pNIPAM (yellow) and pAAM (green) tubes recorded at different temperatures. Scale bars indicate 1 cm.

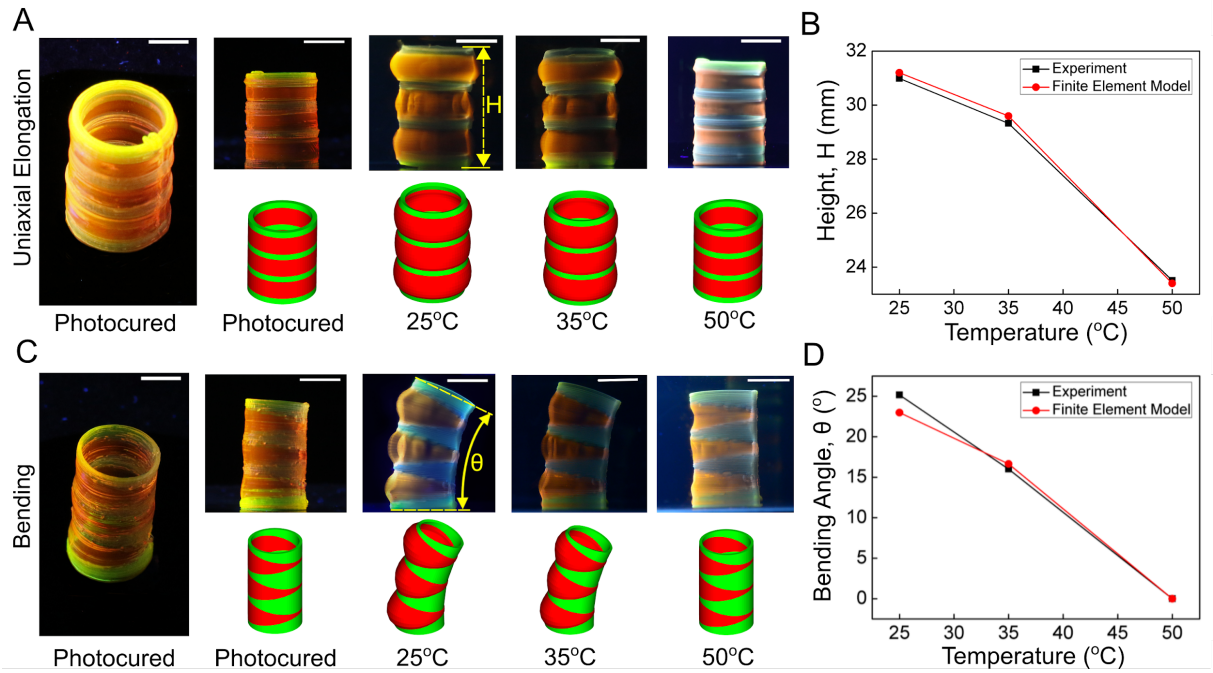

Figure 2. Bilaterally symmetric tubes with horizontal, periodically-spaced segments. (A-B) Results showing thermoresponsive uniaxial elongation of tubes with alternating cylindrical discs of active pNIPAM (red) and passive pAAM (green) segments. **(A)** Optical and FEA snapshots of shape change of tubes at different temperatures. H indicates the height of the tube which is plotted against temperature in panel (**B**). **(C- D)** Results showing thermoresponsive bending of tubes with alternating cylindrical wedge-shaped segments of active pNIPAM (red) and passive pAAM (green) segments. **(C)** Optical and FEA snapshots of shape change of tube at different temperatures. θ indicates the bending angle of the tube which is plotted against temperature in panel (**D**). The experimental snapshots of all tubes were obtained after soaking them in water while heating and allowed to equilibrate at the desired temperature over 24 hours. The simulation snapshots and plots agree with the experiments. The printing of tube designs was repeated multiple times and no significant variation was observed (we estimate less than 10%) in height and bending angle change. All scale bars are 1 cm.

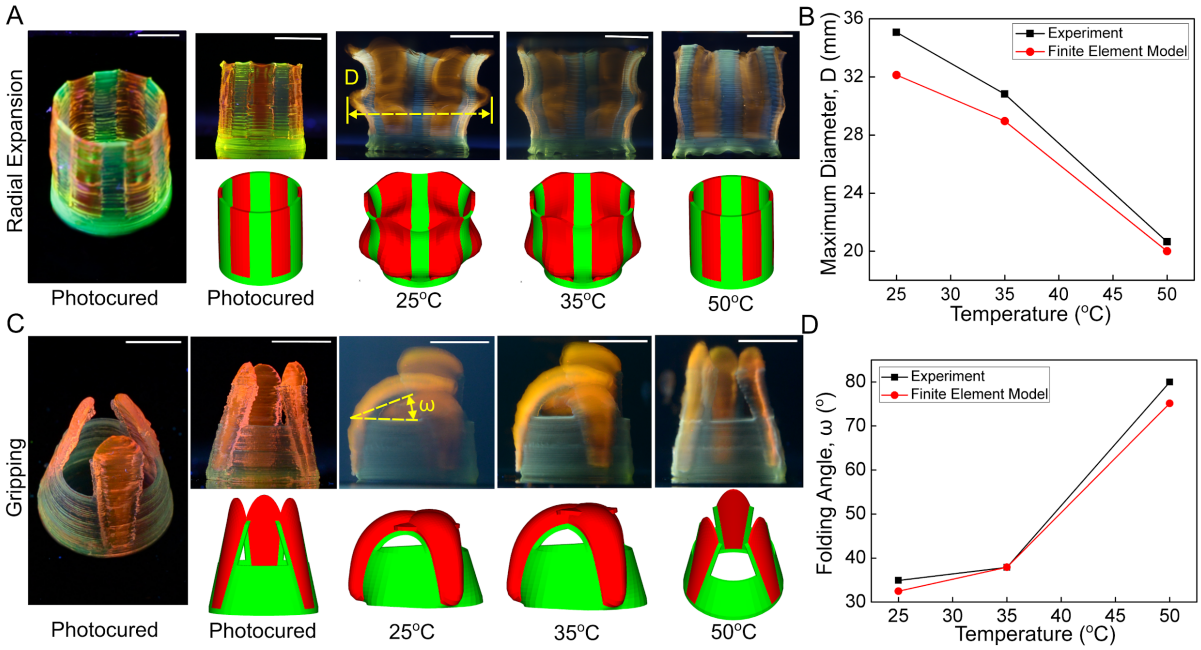

Figure 3. Radially symmetric tubes with vertical, periodically-spaced segments. (A- B) Results showing thermoresponsive radial expansion of tubes with alternating vertical segments of active pNIPAM (red) and passive pAAM (green) segments. **(A)** Optical and FEA snapshots of shape change of tubes at different temperatures. D indicates the diameter of the tube at the point of maximal expansion which is plotted against temperature in panel (**B**). **(C-D)** Results showing thermoresponsive folding of fingers on tubes with vertical segments of active pNIPAM (red) and passive pAAM (green) segments. **(C)** Optical and FEA snapshots of shape change of the tube at different temperatures. ω indicates the folding angle of the fingers which is plotted against temperature in panel (**D**). The experimental snapshots of all tubes were obtained after soaking them in water while heating and allowed to equilibrate at the desired temperature over 24 hours. The simulation snapshots and plots agree with the experiments. All scale bars are 1 cm.

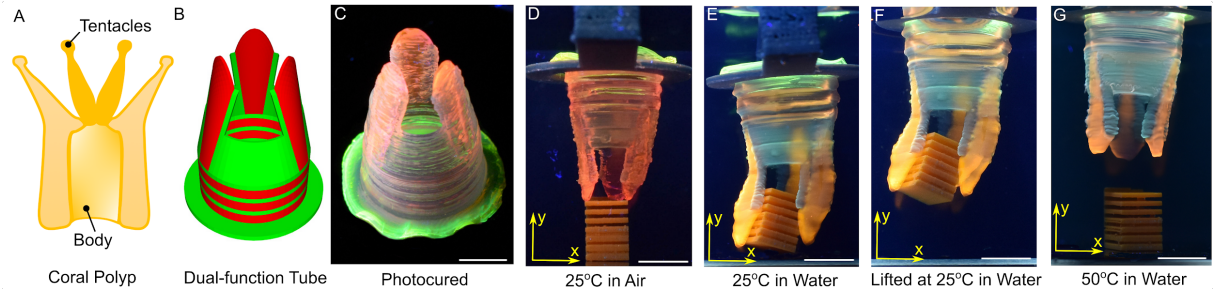

Figure 4. Dual-shape change tubes. (A) Schematic of the basic anatomy of the coral polyp; the image was created based on encyclopedic depictions of the polyp.[50] **(B-C)** CAD model and image of a 3D printed and photocured tube with cylindrical base and three fingers. **(D-G)** Optical snapshots of shape change of the tube at different temperatures. The tube was suspended over a part placed in a tank. When water was added to the tank, the tube shows uniaxial elongation and gripping of the part. Upon heating to 50°C, the tube shortened and the fingers opened to release the part back to the bottom of the tank. Scale bars are 1 cm.

TOC

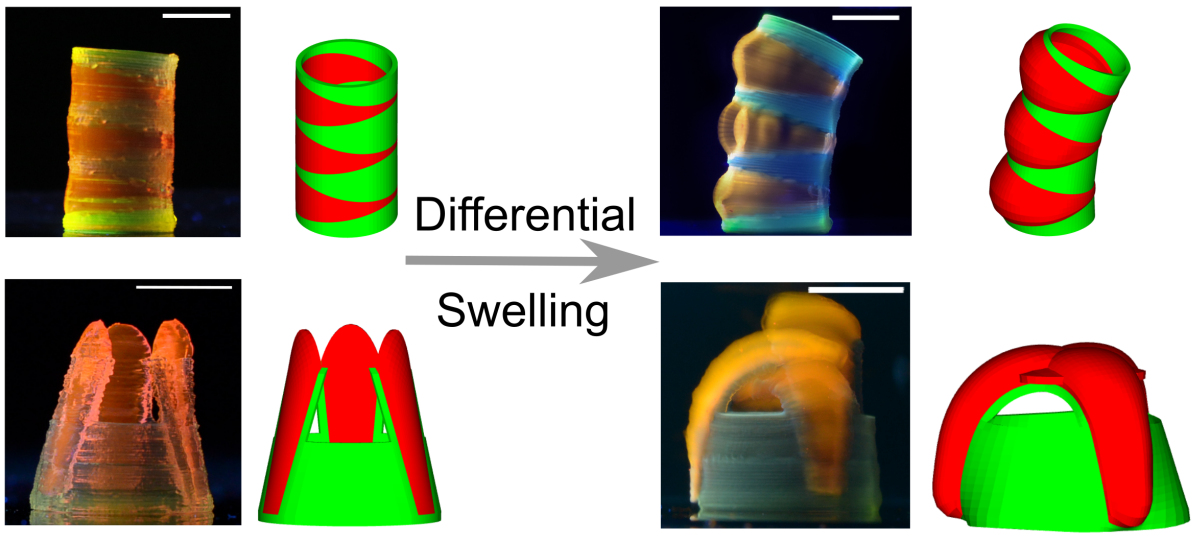

Supporting Information

Dual-gel 4D Printing of Bioinspired Tubes

Jiayu Liu[1], Ozan Erol[1,2,3], Aishwarya Pantula[3], Wangqu Liu[3], Zhuoran Jiang[3], Kunihiko Kobayashi[9], Devina Chatterjee[3], Narutoshi Hibino[5], Lewis H. Romer[6,7], Sung Hoon Kang[1,2,8], Thao D. Nguyen[1,2] and David H. Gracias[3,4,]*

[1] Department of Mechanical Engineering, Johns Hopkins University, 3400 N Charles Street, Baltimore, MD 21218, USA
[2] Hopkins Extreme Materials Institute, 3400 N Charles Street, Baltimore,Johns Hopkins University, Baltimore, MD 21218, USA
[3] Department of Chemical & Biomolecular Engineering, Johns Hopkins University, 3400 N Charles Street, Baltimore,Baltimore, MD 21218, USA
[4] Department of Materials Science and Engineering, Johns Hopkins University, 3400 N Charles Street, Baltimore, Baltimore, MD 21218, USA
[5] Division of Cardiac Surgery, Department of Surgery, 1800 Orleans Street, Johns Hopkins Hospital, Baltimore, MD 21287, USA
[6] Departments of Anesthesiology and Critical Care Medicine, Cell Biology, Pediatrics, Johns Hopkins University School of Medicine, 1800 Orleans Street, Baltimore, MD 21287, USA
[7] Biomedical Engineering and the Center for Cell Dynamics, Johns Hopkins University School of Medicine, 1800 Orleans Street, Baltimore, MD 21287, USA
[8] Institute for NanoBioTechnology, Johns Hopkins University, 3400 N Charles Street, Baltimore, Baltimore, MD 21218, USA
[9] JSR Corporation, 1-9-2, Higashi-Shimbashi, Minato-ku, Tokyo 105-8640, Japan

*Corresponding author: dgracias@jhu.edu

Note S1: Note on Experimental Details for Dual-gel 3D Printing.

The general procedure for creating dual-hydrogel 3D structures involved three steps; (a) preparation of active and passive inks, (b) 3D printing of structures, and (c) Ultraviolet (UV) photocuring of structures. After photocuring, the structures were soaked in deionized water (DI water) at the desired temperature for 24 hours to allow swelling and shape transformations to equilibrate.

Preparation of active (NIPAM) and passive (AAM) inks.

Our active ink contained a monomer (NIPAM), shear-thinning agent (Laponite nanoclay), photoinitiator (Irgacure 2959), dye, and DI water. Our passive ink contained a monomer (AAM), shear-thinning agent (Laponite nanoclay), photoinitiator (Irgacure 2959), chemical crosslinker (BIS), dye, and DI water. The mixing process of the active and passive inks is presented in the methods section of the main text. After mixing, the inks were transferred into UV-shielding cartridges and centrifuged at 2100 rpm for 90 seconds to remove air bubbles. Then, they were allowed to rest for a minimum of 24 hours for the hydration process to achieve the desired shear thinning property.

3D printing of structures.

We used the Cellink Inkredible+ bioprinter for the 3D printing process. Print paths were generated via g-code which outputs the XYZ motion of the two print heads. All the CAD and STL files for the dual-hydrogel modules were created in Solidworks (Dassault Systèmes), and the g-code files were generated using the Slic3r software with a layer height of 0.4 mm.

Printing tall structures of dual-materials requires a number of challenges to be overcome. First, switching between the two materials needs to be seamless, which necessitates that the two nozzle tips be perfectly aligned with each other. Even a small misalignment of the nozzles accumulates recurring errors in each layer resulting in significant defects in the final structure. Moreover, printing 3D tall structures is more technically demanding than printing shorter 2D structures. The tall structures we printed require approximately 50-100 layers of printing, and a single perturbation (such as an air bubble or clog) in the printing process ruins the entire print.

Essentially our 3D printing process consisted of two steps: calibration and printing.

Calibration: First, we made sure that both print heads were levelled with each other in the Z direction. Then, for calibration in the X and Y directions, we printed a calibration structure consisting of a pNIPAM tube on top of a pAAM tube. The objective of this step was to check whether there was any misalignment between the two print heads, because even a small misalignment will accumulate recurring errors in each layer, resulting in defects in the structure and undesired shape change. If any misalignments were observed, we added preset values in the X and Y directions for the print heads in the g-code files. This step was repeated multiple times until the print heads were perfectly aligned to ensure seamless printing of the

two inks.

Printing: The cartridges were attached to the 3D Printer and connected to air pump pressure control. We used 27G nozzles (diameter 0.41 mm) for continuous printing without any clogging. The structures were 3D printed on a silicon wafer in air at room temperature. We optimized the printing pressures of the active and passive inks for the printing speed of 10 mm s^{-1}. The pressures used for printing active and passive inks were 90-100 kPa and 110-130 kPa respectively.

UV curing of horizontal and vertical gel segments.

After 3D printing, the structures were UV photocured to crosslink the active and passive hydrogels. Uniform UV curing of tall 3D structures was essential to achieve the desired shape change. While many researchers cure their structures from above, we found that this strategy resulted in significant crosslink gradients. We established a new rotating platform which facilitated the uniform photocrosslinking of the entire structure. We placed the 3D printed structures in the center of a table that was rotated at 9.6 rpm, and used the LX 500 Omnicure system (Lumen Dynamics) with two UV LED heads (wavelength 365 nm) for the curing process. Each UV head was equipped with a lens of diameter 12 mm and pointed towards the surface of the structures at a distance of 3 cm. The homogeneous pNIPAM tubes and pAAM tubes (Figure 1B) were cured as a single section. The other segmented tubes (Figure 2 - Figure 4) were photocured section-by-section depending on the structural height, and each section was cured for 9 mins to ensure the photocrosslinking of active and passive hydrogels. For the uniaxial elongation tube, bending tube, radial expansion tube, and gripper, the top and bottom sections were cured successively. The coral polyp inspired dual-shape change tube was cured as three sections.

Macro-imaging of 3D gel tubes.

The images of all the tubes were taken using a Canon EOS 70D digital camera with a variety of lenses. A broad spectrum UV light source (Spectroline Model EF-160C, Spectronics Corporation, USA) was used to excite the fluorescent dye in the tubes. After 3D printing and photocuring, images of the photocured tubes were taken in air at room temperature.

The tubes were then immersed in DI water and kept in an incubator (MODEL 1575, Sheldon Manufacturing, INC., USA) set at the desired testing temperatures for at least 24 hours to reach their equilibrium swollen state. The pictures of tube shape change were taken in DI water at the corresponding temperatures. We started the time-lapse study of the tubes after immersion in DI water at room temperature. We connected the Pixel T3/E3 Timer Shutter Release Remote Control to the camera and took pictures every 50 seconds for 6 hours.

Note S2: Finite Element Model.

Various theoretical hydrogel models have been developed in recent years to explain the coupled mechanical and stimuli responsive swelling behavior of hydrogels and to guide the design of hydrogel composite structures.[1,2] We previously described a constitutive model for thermoresponsive hydrogels that can accurately predict their equilibrium shapes at different temperatures.[3–5] In our model, we neglected the kinetics of diffusion and assumed that the hydrogel remained in equilibrium throughout the deformation. This is a reasonable approximation since in our experiments, we keep the hydrogel structures in DI water at the desired temperature for at least 24 hrs so that it can reach its equilibrium state.

In the constitutive model, we first defined a deformation field $\mathbf{x} = \varphi(\mathbf{X})$, that maps from material points $\mathbf{X}$ in the initial undeformed dry polymer configuration to spatial points $\mathbf{x}$ in the current deformed hydrogel configuration. The total deformation gradient tensor $\mathbf{F}$ was defined as $\mathbf{F} = \partial\mathbf{x}/\partial\mathbf{X}$. To model the stress-free swelling of the hydrogel, the total deformation gradient tensor was further decomposed into two parts: a swelling part $\mathbf{F_s}$ and a mechanical part $\mathbf{F_e}$,

$$\mathbf{F} = \mathbf{F_e}\mathbf{F_s}, \tag{S1}$$

where $\mathbf{F_s} = \phi^{-1/3}\mathbf{I}$. ϕ is the polymer volume fraction of the hydrogel and defined as $\phi = 1/(1+\nu c)$, where ν is the volume per solvent molecule and c is the number of solvent molecules per polymer volume. We defined the stress-free swollen configuration as the reference configuration, and a deformation gradient tensor $\mathbf{f}$ mapping from the stress-free reference configuration to the final deformed configuration:

$$\mathbf{f} = \phi_0^{1/3}\mathbf{F}, \tag{S2}$$

where φ_0 is the polymer volume fraction of the hydrogel in the reference configuration. The left Cauchy-Green deformation tensor was defined as $\mathbf{b} = \mathbf{F}\mathbf{F}^{\mathbf{T}}$. We expressed the $\mathbf{b}$ tensor in terms of its principle stretches λ_i and principle directions $\mathbf{n_i}$:

$$b = \sum_{i=1}^{3} \lambda_i^2 \, n_i \otimes n_i, \tag{S3}$$

and the corresponding principal stretches of $\mathbf{f}$ tensor are $\overline{\lambda_i} = \phi_0^{1/3}\lambda_i$. The change of volume of the entire deformation process from the dry polymer configuration to the final hydrogel configuration was related to the mechanical part and swelling part as: $J=\det[\mathbf{F}]=\det[\mathbf{F_e}]\det[\mathbf{F_s}]=J_e\,\phi^{-1}$.

We assumed that the free energy density of the hydrogel could be additively decomposed into two terms: a mechanical term arising from the stretching of a polymer network and a mixing term arising from the mixing of the polymer network and solvent:

$$\Psi = \Psi_{mechanical}(I_b, J_e) + \Psi_{mixing}(\phi), \tag{S4}$$

where I_b is the first invariant of $\mathbf{b}$ tensor: $I_b = \mathrm{tr}[\mathbf{b}]$.

We used the quasi-incompressible Neo-Hookean model to model the strain energy density of the polymer network with Gaussian chain statistics:

$$\Psi_{mechanical}(I_b, J_e) = \frac{G}{2}(I_b - 3 - 2logJ) + \frac{K}{4}(J_e^2 - 2logJ_e - 1), \quad \text{(S5)}$$

where G and K are the shear modulus and bulk modulus of the polymer network respectively. To achieve the volumetric incompressibility of mechanical deformation, we assumed that the bulk modulus is 1000 times of the shear modulus.

We used the Flory-Huggins model[6] to describe the free energy density of mixing:

$$\Psi_{mixing}(\phi) = \frac{RT}{v\phi}[(1-\phi)log(1-\phi) + \chi\phi(1-\phi)], \quad \text{(S6)}$$

where R is the gas constant, T is the temperature, and χ is the Flory-Huggins interaction parameter. To model the thermoresponsive behavior, we assumed that the Flory–Huggins interaction parameter had the following form,[7]

$$\chi = \frac{1}{2}(\chi_L + \chi_H) + \frac{1}{2}(\chi_H - \chi_L)tanh(\frac{T - T_{tran}}{\Delta T}), \quad \text{(S7)}$$

where χ_L and χ_H are the Flory-Huggins interaction parameters at low and high temperatures respectively, T_{tran} is the transition temperature, and ΔT is the width of transition region.

We calculated the Cauchy stress tensor from hyperelasticity theory as $\boldsymbol{\sigma} = (1/J)(\partial\Psi/\partial\mathbf{F})\mathbf{F}^{\mathbf{T}}$, and we obtained the chemical potential using thermodynamics arguments as $\mu = \partial\Psi/\partial c$, where c is the number of solvent molecules per polymer volume. By substituting equations (S4)~(S6) into the above two relations, we obtained the equations of state for the hydrogel model:

$$\sigma = \sum_{i=1}^{3}\{\frac{G\phi_0}{\lambda_1\lambda_2\lambda_3}(\phi_0^{-2/3}\overline{\lambda_i^2} - 1) + \frac{K\phi_0}{2\lambda_1\lambda_2\lambda_3}[(\frac{\phi}{\phi_0}\overline{\lambda_1}\,\overline{\lambda_2}\,\overline{\lambda_3})^2 - 1]\}n_i \otimes n_i, \quad \text{(S8)}$$

$$\mu = RT[log(1-\phi) + \phi + \chi\phi^2] - \frac{Kv\phi}{2}[(\frac{\phi}{\phi_0}\overline{\lambda_1}\,\overline{\lambda_2}\,\overline{\lambda_3})^2 - 1]. \quad \text{(S9)}$$

The hydrogel constitutive model was implemented into TAHOE (Sandia National Laboratories) for finite element simulation of hydrogel structures. The parameters of the hydrogel constitutive model are as follows: polymer shear modulus G, and χ_L, χ_H, T_{tran}, ΔT which determine the thermo-responsive swelling of hydrogel.

Determination of model parameters.

Active hydrogel:

We used the hydrogel constitutive model derived above to describe the thermoresponsive swelling of pNIPAM hydrogel. We 3D printed pNIPAM hydrogel square plates of side length 10 mm and thickness 2 mm to measure the elastic modulus of the hydrogel. After photocuring, the hydrogel samples were placed into DI water at room temperature for 24 hours to reach the free swollen equilibrium state. We used a DMA (Dynamic Mechanical Analyzer Q800, TA Instruments) to carry out unconfined compression tests on the hydrogel samples with a maximum applied static force of 6 mN at a rate of 1 mN min^{-1}. The static force and displacement data output from the DMA were converted to engineering stress and engineering strain. We tested three pNIPAM hydrogel square plate samples and calculated the average Young's modulus $E_{pNIPAM}^{Gel} =$ 2.53 kPa from the slopes of engineering stress-engineering strain curves (Figure S3(A)), which corresponds to a shear modulus of $G_{pNIPAM}^{Gel} = \frac{1}{3}E_{pNIPAM}^{Gel} = 0.84\ kPa$ assuming mechanical incompressibility.

We measured the volumetric swelling ratio of the active hydrogel from the dry state to the equilibrium swollen state at room temperature to calculate the polymer's elastic modulus. We first measured the average weight $M_{hydrated}$ of three pNIPAM square plate hydrogel samples in the equilibrium swollen state at room temperature. The hydrogel samples were then put into incubator (MODEL 1575, Sheldon Manufacturing, INC., USA) in air at 50°C for 24 hours to reach completely dry state, and weighted again (M_{dry}). The volumetric swelling ratio of pNIPAM hydrogel from the dry state to the equilibrium swollen state at room temperature was calculated by $Q_{pNIPAM} = M_{hydrated}/M_{dry} = 21.14$. The pNIPAM polymer shear modulus $G_{pNIPAM}^{Polymer}$ is related to the hydrogel shear modulus as:[3] $G_{pNIPAM}^{Polymer} = G_{pNIPAM}^{Gel} \times Q_{pNIPAM}^{1/3} = 2.32\ kPa.$

We conducted a swelling test on the homogeneous 3D printed pNIPAM hydrogel tubes (main text Figure 1(B)) to determine the remaining parameters in the model. After photocuring, the three pNIPAM hydrogel tubes were placed into DI water in the incubator at 50°C, 41°C, 33°C, 25°C, 33°C, 41°C, and 50°C for 24 hours to reach the equilibrium state at each temperature. We took optical images of the pNIPAM hydrogel tubes at different temperatures, and measured the average tube outer diameter D using the ImageJ software. We plotted the fractional change in diameter ($\Delta D/D_0$) of the pNIPAM hydrogel tubes at different temperatures in main text Figure 1(B), where D_0 represents the average pNIPAM tube outer diameter in the photocured state, and ΔD represents the average change of outer diameter under different temperatures. The parameters χ_L, χ_H, T_{tran}, ΔT were obtained by fitting the simulation free swelling data to the experimental results in main text Figure 1(B). The model parameters for the active pNIPAM hydrogel are summarized in Table S1.

Passive hydrogel:

We conducted all of the same experiments described above on the passive pAAM hydrogel. The $\Delta D/D_0$ of the 3D printed pAAM hydrogel tubes at different temperatures were plotted in main text Figure 1(B). We observed that the swelling of the pAAM hydrogel tubes was negligible ($\Delta D/D_0 = 1.2\%$), and independent of temperature. Hence, we used the quasi-incompressible Neo-Hookean model to describe the passive pAAM hydrogel.

We conducted unconfined compression tests on three 3D printed pAAM hydrogel square plate samples with a maximum applied strain of 5% at a rate of 0.1% s^{-1}. We calculated the average hydrogel Young's modulus $E_{pAAM}^{Gel} = 60.3\ kPa$ from the engineering stress-engineering strain curves (Figure S3(B)), which corresponds to a hydrogel shear modulus of $G_{pAAM}^{Gel} = \frac{1}{3}E_{pAAM}^{Gel} = 20.1\ kPa$ assuming mechanical incompressibility. We measured the volumetric swelling ratio of the passive hydrogel samples from the dry state to the equilibrium swollen state at room temperature ($Q_{pAAM} = 5.57$), and calculated the pAAM polymer shear modulus: $G_{pAAM}^{Polymer} = G_{pAAM}^{Gel} \times Q_{pAAM}^{1/3} = 35.63\ kPa.$

Note S3: Finite Element Simulations for Horizontal and Vertical Gel Segments.

The finite element models of the horizontal and vertical gel segments are shown in Figure S4. The dimensions of each model geometry were the same as measured from the structures' experimental pictures in the photocured state. The mesh was discretized using trilinear hexahedral elements. As boundary conditions, one point of the structure's bottom plane was fixed. The displacement boundary conditions of the uniaxial elongation tube and the radial expansion tube were set as:

$$\begin{aligned} u_x(x = 10,\ y = 0,\ z = 0) &= 0, \\ u_y(x = 10,\ y = 0,\ z = 0) &= 0, \\ u_z(x = 10,\ y = 0,\ z = 0) &= 0. \end{aligned} \tag{S10}$$

The displacement boundary conditions of the bending tube were set as:

$$\begin{aligned} u_x(x = 7.5,\ y = 0,\ z = 0) &= 0, \\ u_y(x = 7.5,\ y = 0,\ z = 0) &= 0, \\ u_z(x = 7.5,\ y = 0,\ z = 0) &= 0. \end{aligned} \tag{S11}$$

The displacement boundary conditions of the gripper were set as:

$$\begin{aligned} u_x(x = 9,\ y = 0,\ z = 0) &= 0, \\ u_y(x = 9,\ y = 0,\ z = 0) &= 0, \\ u_z(x = 9,\ y = 0,\ z = 0) &= 0. \end{aligned} \tag{S12}$$

The simulations started from the photocured state. The initial polymer fraction φ_0 was obtained by solving equation (S8) and (S9) with the condition $\boldsymbol{\sigma} = 0$ and $\mu = 0$. The model temperature was continuously increased to different temperatures (25°C, 35°C, and 50°C) to predict the equilibrium shape changes of the structures. At each temperature, the deformation gradient **f** and polymer volume fraction φ were updated to satisfy the momentum balance and chemical potential equilibrium.

References:

(1) Hong, W.; Zhao, X.; Zhou, J.; Suo, Z. A Theory of Coupled Diffusion and Large Deformation in Polymeric Gels. *J. Mech. Phys. Solids* **2008**, *56* (5), 1779–1793.

(2) Chester, S. A.; Anand, L. A Coupled Theory of Fluid Permeation and Large Deformations for Elastomeric Materials. *J. Mech. Phys. Solids* **2010**, *58* (11), 1879–1906.

(3) Yoon, C.; Xiao, R.; Park, J.; Cha, J.; Nguyen, T. D.; Gracias, D. H. Functional Stimuli Responsive Hydrogel Devices by Self-Folding. *Smart Mater. Struct.* **2014**, *23* (9), 094008.

(4) Breger, J. C.; Yoon, C.; Xiao, R.; Kwag, H. R.; Wang, M. O.; Fisher, J. P.; Nguyen, T. D.; Gracias, D. H. Self-Folding Thermo-Magnetically Responsive Soft Microgrippers. *ACS Appl. Mater. Interfaces* **2015**, *7* (5), 3398–3405.

(5) Guo, J.; Shroff, T.; Yoon, C.; Liu, J.; Breger, J. C.; Gracias, D. H.; Nguyen, T. D. Bidirectional and Biaxial Curving of Thermoresponsive Bilayer Plates with Soft and Stiff Segments. *Extreme Mechanics Letters* **2017**, *16*, 6–12.

(6) Flory, P. J.; Rehner, J. Statistical Mechanics of Cross‐Linked Polymer Networks II. Swelling. *J. Chem. Phys.* **1943**, *11* (11), 521–526.

(7) Chester, S. A.; Anand, L. A Thermo-Mechanically Coupled Theory for Fluid Permeation in Elastomeric Materials: Application to Thermally Responsive Gels. *J. Mech. Phys. Solids* **2011**, *59* (10), 1978–2006.

Supplementary Figures

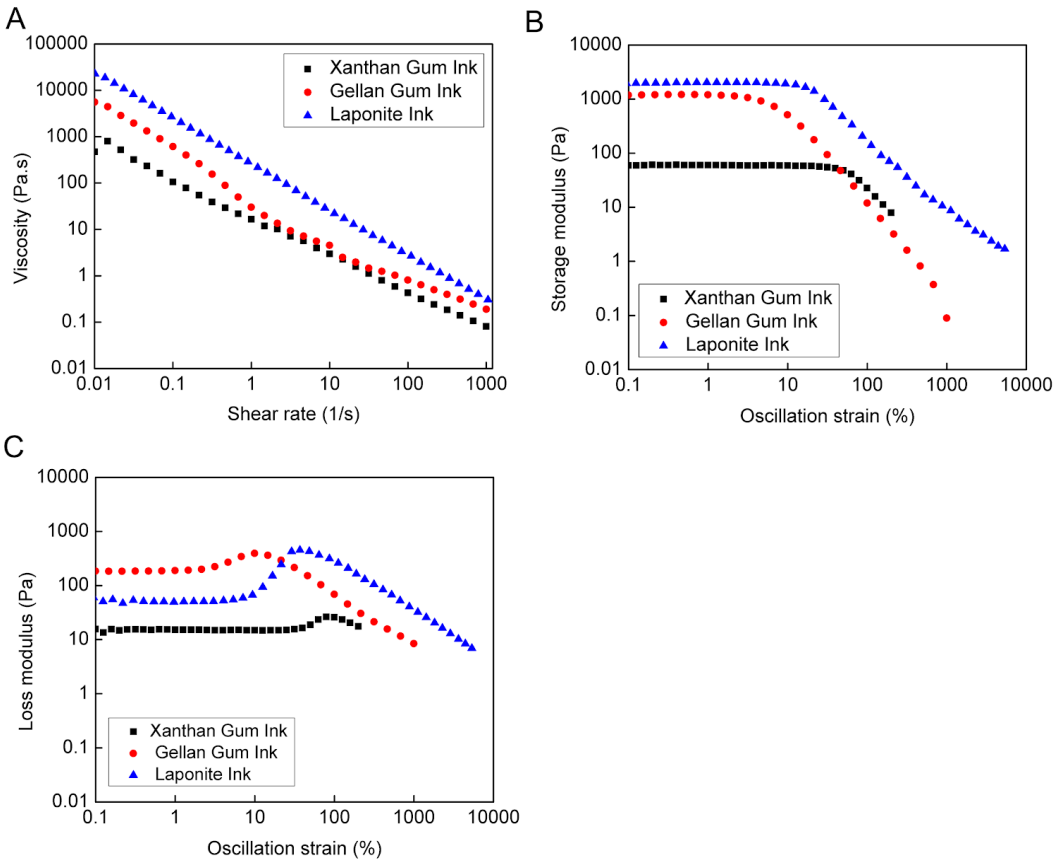

Figure S1. Rheological measurements of the NIPAM inks. Log-log plots of, (**A**) Ink viscosity as a function of shear rate of NIPAM ink blended with Xantham gum, Gellan gum and Laponite, (**B**) Storage modulus as a function of oscillation strain, and (**C**) loss modulus as a function of oscillation strain for NIPAM inks blended with different shear thinning agents: (black) 3 wt% Xanthan gum ink, (red) 2 wt% Gellan gum ink, and (blue) 6.77 wt% Laponite ink.

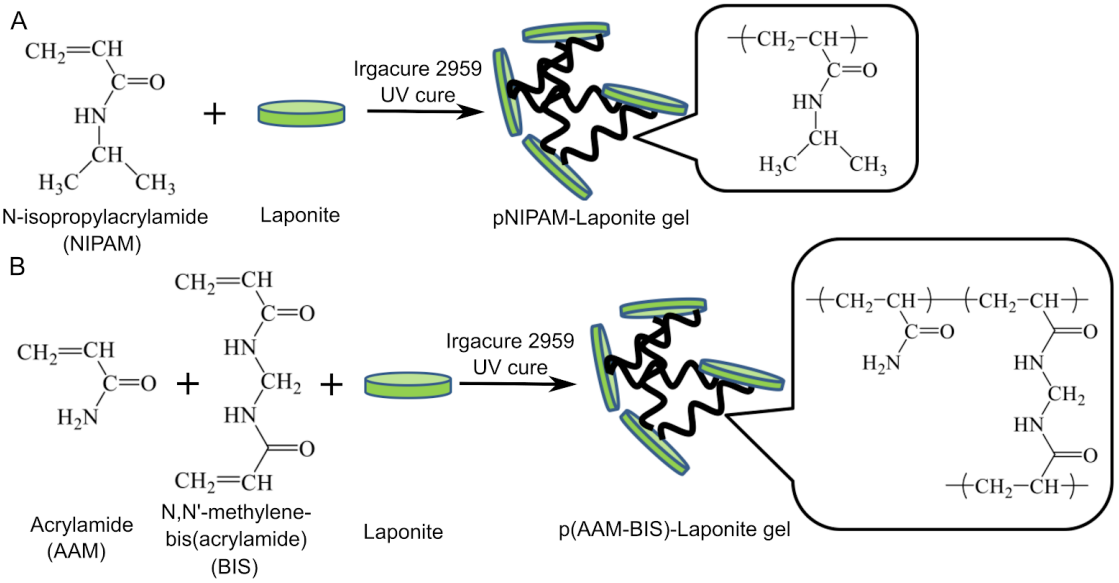

Figure S2. Schematic representation of the molecular and microstructure of the inks. (A) active NIPAM ink and (B) passive AAM ink.

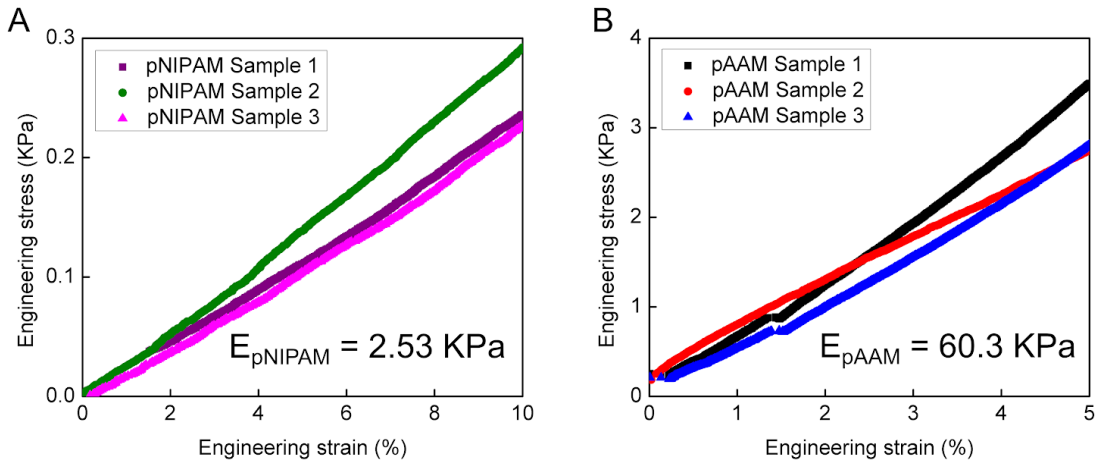

Figure S3. Results of stress-strain measurements of 3D printed and photocured pNIPAM and pAAM hydrogels. Elastic moduli measurements were obtained for fully hydrated hydrogel square plates to determine the stiffness of the active and passive hydrogels used in this study. (**A**) The elastic modulus of the pNIPAM gel sample was measured using unconfined compression test at room temperature (DMA Q800; TA instruments) with a maximum applied static force of 6 mN at a rate of 1 mN min^{-1}. (**B**) The elastic modulus of the pAAM gel sample was measured using unconfined compression test at room temperature with a maximum applied strain of 5% at a rate of 0.1% s^{-1}. Static force and displacement data of the compression test were used to generate engineering stress and engineering strain curves. The elastic modulus was measured as the slope of the best-fit line to the stress-strain curves.

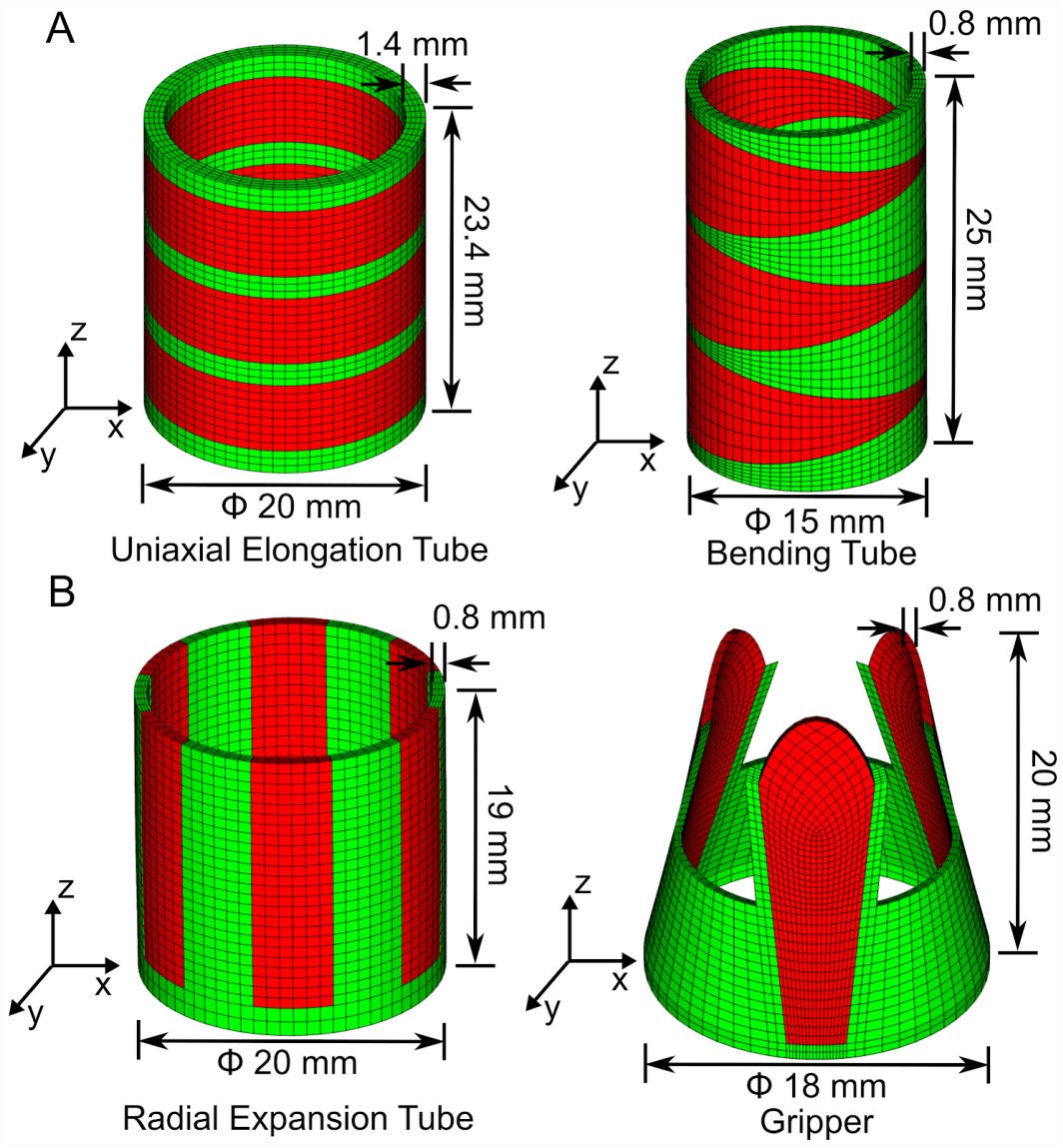

Figure S4. Finite element model snapshots of the functional dual-gel tubes. (**A**) Horizontal gel segments, and (**B**) Vertical gel segments. Green represents passive pAAM hydrogel and red represents active pNIPAM hydrogel. The model geometries are the same as those measured experimentally in the photocured state.

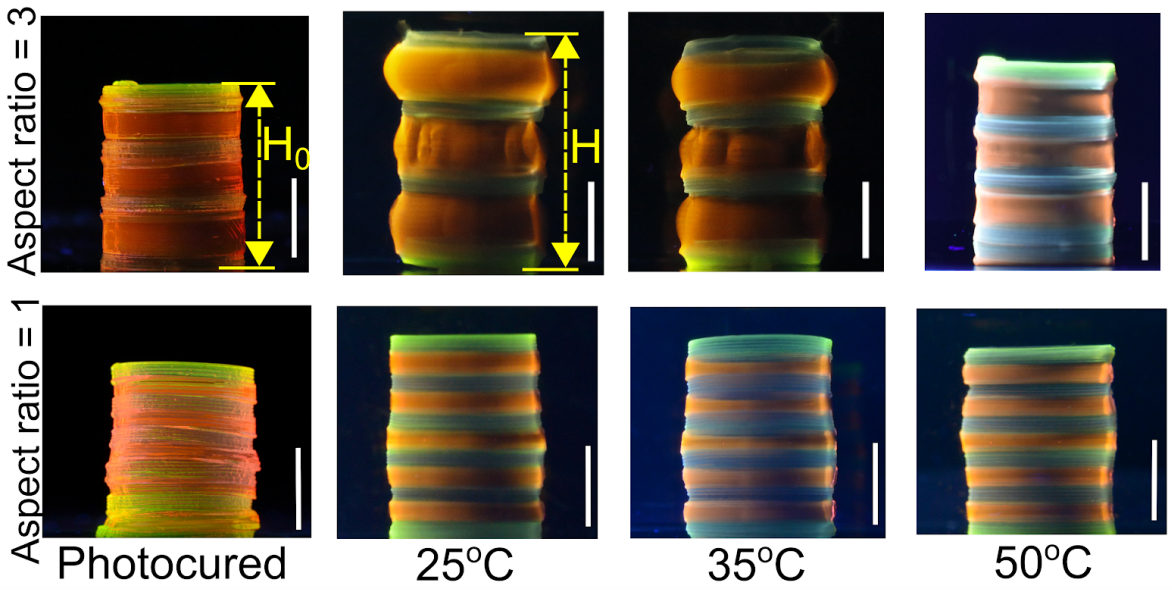

Figure S5. Shape change snapshots of the uniaxial elongation tube with different aspect ratios ($\frac{h_{pNIPAM}}{h_{pAAM}}$). h_{pNIPAM} and h_{pAAM} represent the height of the active and passive rings respectively. Increasing the aspect ratio from 1 (**bottom**) to 3 (**top**) resulted in an increase of elongation ($\frac{H-H_0}{H_0}$) from 15.5% to 32.4%. Scale bars are 1 cm.

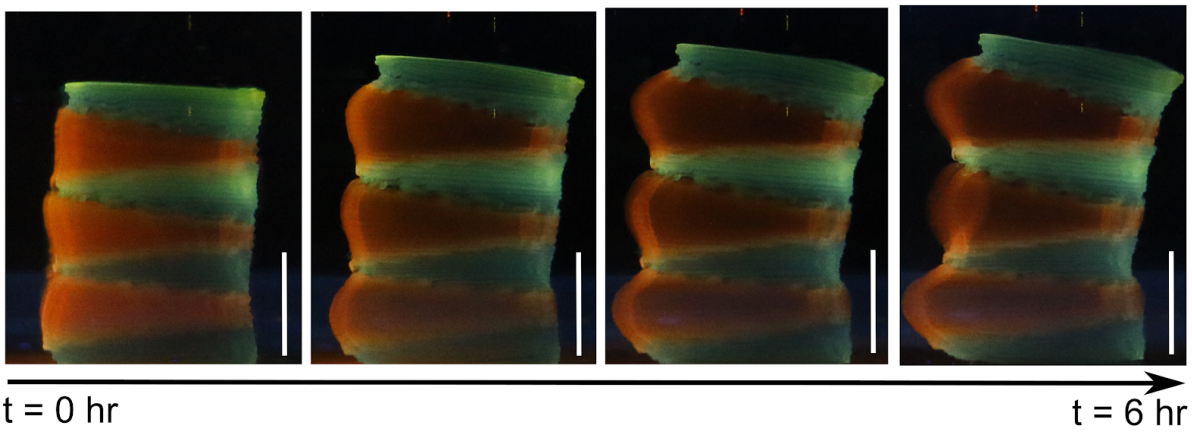

Figure S6. Time-lapse shape change snapshots of the bending tube in DI water at room temperature. Scale bars are 1 cm.

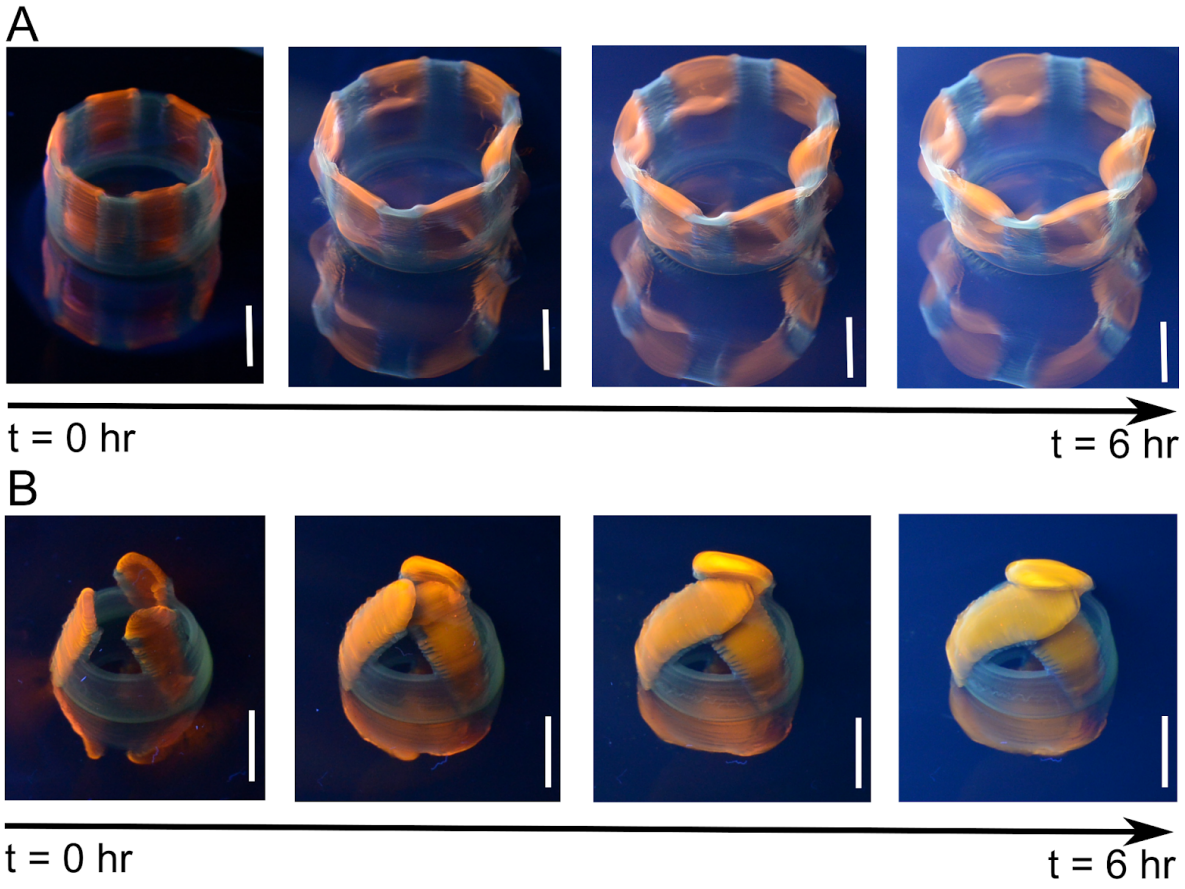

Figure S7. Time-lapse shape change snapshots of the (A) radial expansion tube, and (B) the gripper in DI water at room temperature. Scale bars are 1 cm.

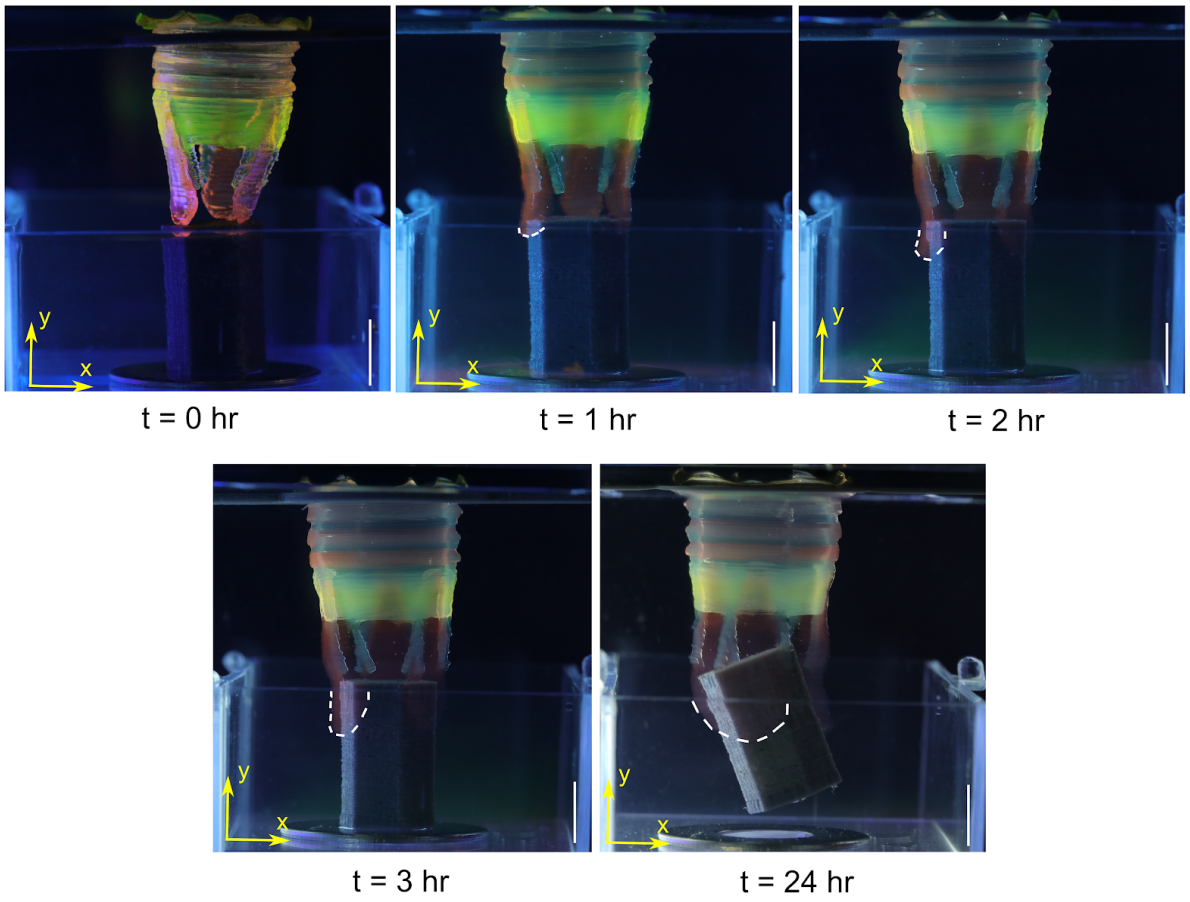

Figure S8. Time lapse of the coral polyp inspired dual-shape change tube reaching inside a box to grab a hexagonal prism. The shape change occurred in DI water at room temperature. Scale bars are 1 cm.

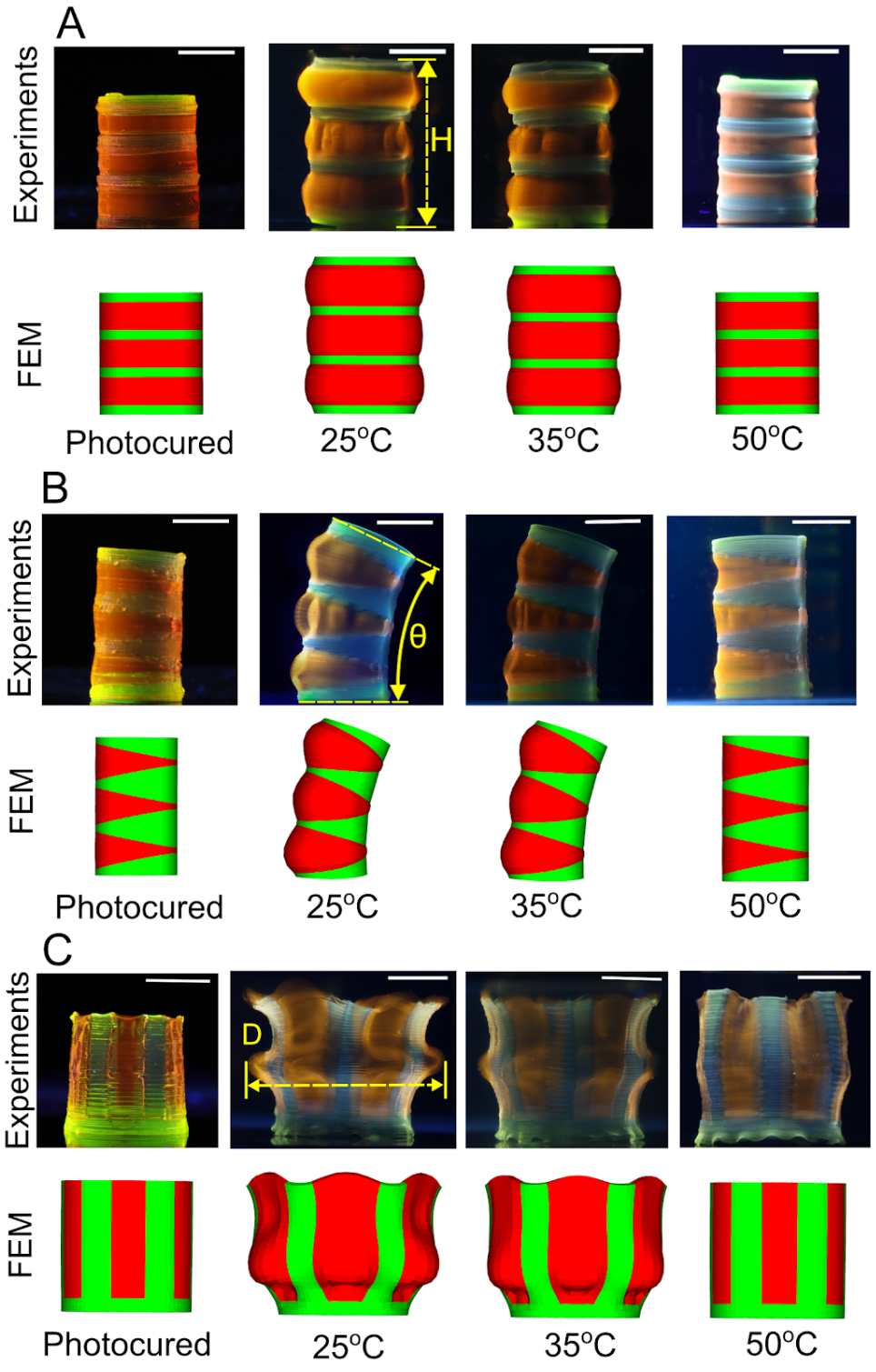

Figure S9. Side-view comparison of experiment results and finite element method (FEM). (**A**) Uniaxial elongation tube, (**B**) Bending tube, and (**B**) Radial expansion tube. Scale bars are 1 cm.

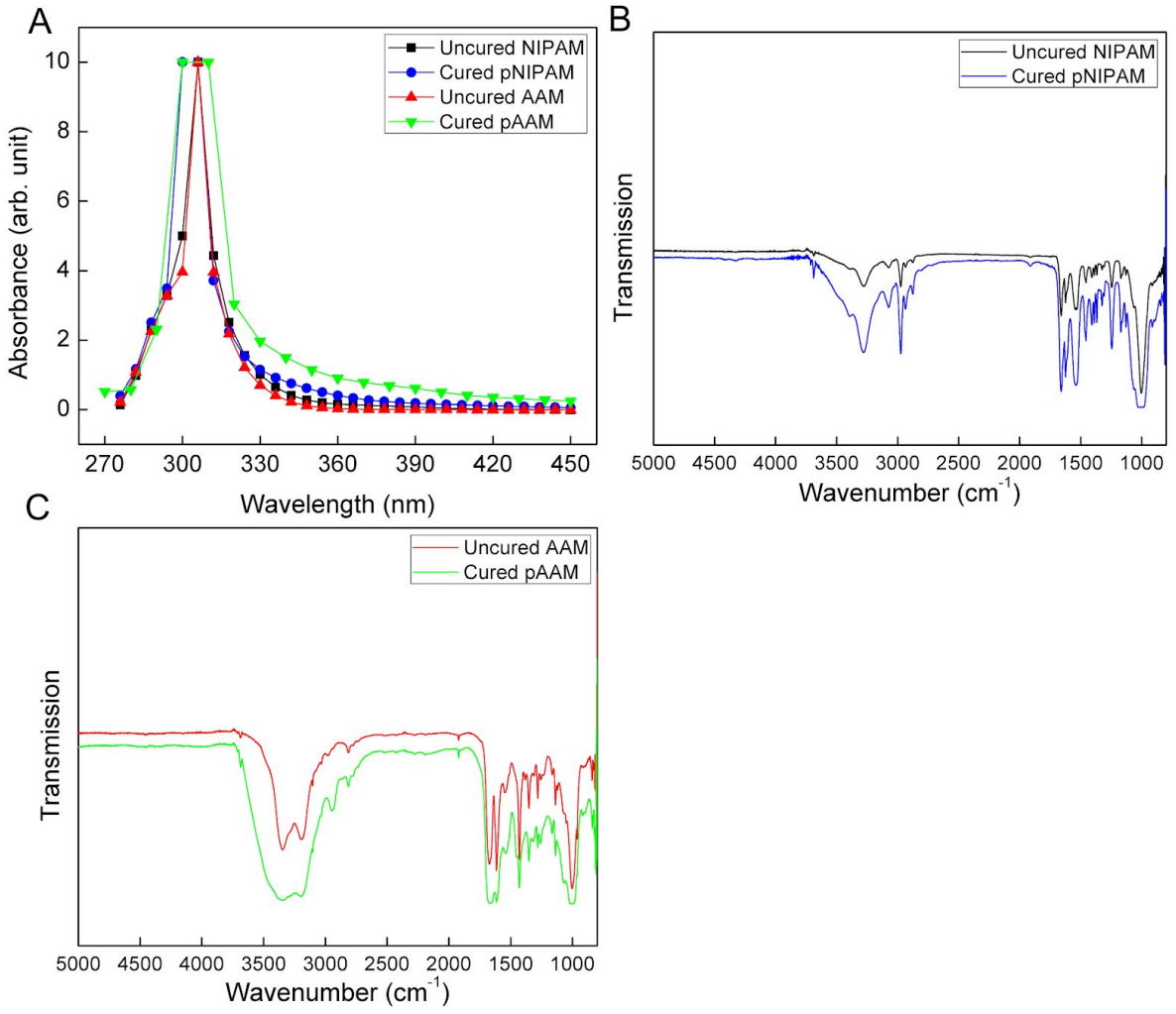

Figure S10. UV-Vis absorbance and FTIR measurements of active and passive inks before and after photocuring. (A) UV-Vis absorption spectra of NIPAM ink and AAM ink before and after photocuring. The inks were transferred into cuvettes and the absorption spectra were measured using a PerkinElmer UV/VIS/NIR Spectrometer Lambda 950 with readings acquired in 6 nm increments. **(B- C)** FTIR spectra of the NIPAM and AAM ink before and after photocuring. The main features are similar with small differences before and after curing. The FTIR spectra were measured using a Bruker Hyperion FTIR Microscope.

G (kPa)	χ_L	χ_H	T_{tran} (°C)	ΔT (°C)
2.32	0.5	0.9	34	4

Table S1. Model parameters determined for the 3D printed active pNIPAM hydrogel